EFFECTS OF BOATTAIL GEOMETRY SMALL CHANGES TO DRAG AT M>1

SERDAREVIC-KADIC, S., SOFTIC, A., RAZIC, F. & TERZIC, J.

Abstract: *This work is focused on numerical simulations of air flow around axisymmetric body in order to determine the effects of boattail geometry on the drag coefficient. Simulations are made for transonic and supersonic speeds of air flow. The influence of boattail geometry to base drag coefficient and drag coefficient of boattail is studied by commercial CFD code FLUENT. Results of simulation are analysed in relation to the image of the velocity field of an original body. The velocity field around the boattail and the base surface are examined to determine the reason for the change in drag due to different boattail geometry. Results show that the minimum drag is around 7° of boattail angle for supersonic flow. The lowest drag coefficient is achieved with longer boattail but it can result in instability which requires additional research.*

Key words: *Boattail, Base, Pressure, Drag, CFD*

Authors´ data: Associate Prof. Dr. Sc. Serdarevic-Kadic S[abina], Associate Prof. Dr. Sc. Softic A[lmira], Assistant Prof. Dr. Sc. Razic F[aruk] & Associate Prof. Dr. Sc. Terzic J[asmin], Faculty of Mechanical Engineering, University of Sarajevo, Vilsonovo setaliste 9,Sarajevo 71000, Bosnia and Herzegovina, serdarevic@mef.unsa.ba, softic@mef.unsa.ba, razic@mef.unsa.ba, terzic@mef.unsa.ba.

This Publication has to be referred as: Serdarevic-Kadic, S[abina]; Softic, A[lmira]; Razic, F[aruk] & Terzic, J[asmin] (2024). Effects of Boattail Geometry Small Changes to Drag at M>1, Chapter 09 in DAAAM International Scientific Book 2024, pp.117-126, B. Katalinic (Ed.), Published by DAAAM International, ISBN 978-3-902734-42-6, ISSN 1726-9687, Vienna, Austria
DOI: 10.2507/daaam.scibook.2024.09

1. Introduction

According to basic sources of aerodynamic force formation, the drag of a body consists of three components: the pressure drag at wet surface, the viscous drag at wet surface and the base drag. The base drag, arising from flow separation at the blunt base of a body, is a considerable part of drag and it can be higher than 50% of the total drag of the body (Sahu, et al., 1997). The remaining part of the drag coefficient includes pressure drag and skin friction drag coefficient.

A properly designed boattail can decrease base drag, regardless of free stream velocity. The addition of a boattail to the base of a heavy-duty vehicle has been shown to generate significant reduction in vehicle drag on the order of 6-12%, resulting in a corresponding reduction in fuel consumption per vehicle (Mcauliffe & Wall, 2016).

Tapering the back of body allows the air to flow along the boattail before separating from the reduced area base (Litz, 2015).

The drag is influenced by a variety of flow and geometrical parameters and with the turbulent boundary layer ahead of the base the major factors acting on base drag include: (1) Mach number in the free stream, just ahead of the base; (2) boundary layer momentum thickness ahead of the base; (3) base diameter; (4) angle of attack; (5) afterbody shape (boattail or flare angle, forebody diameter, afterbody length); and (6) parameters characterising the base drag reduction device (Suliman, et al., 2009).

Streamlines over body of revolution without boattail and with boattail are shown in Fig. 1.

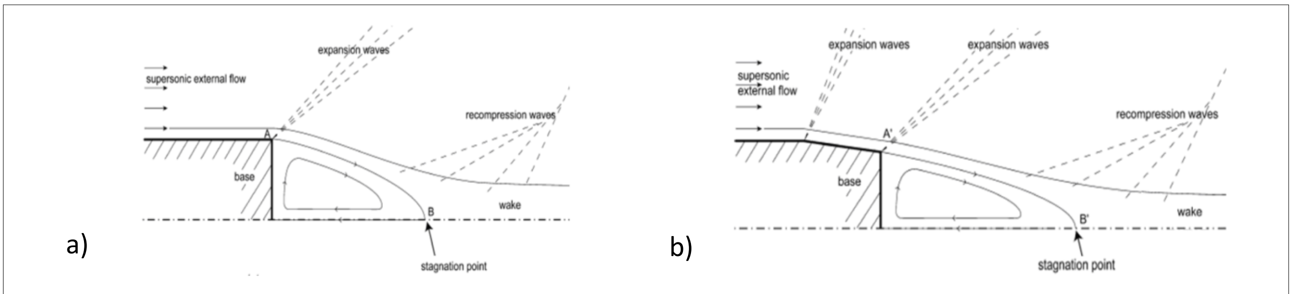

Fig. 1. Streamlines over body of revolution: a) without boattail and b) with boattail (Bournot, et al., 2006)

For bodies of revolution in supersonic flight, the flow field in the wake region has a considerable effect on the aerodynamic drag and small changes in the flow behaviour of the wake may affect the performance of the body.

Fan of expansion waves is formed at edge of base for circular cylinder-body without boattail (Fig. 1.a) in supersonic flow. If body of revolution with boattail (Fig. 1.b) is in supersonic flow, two fans of expansion waves will form. The first fan will generate at the junction between cylinder and boattail and the second fan at the edge of the base. Velocity of flow increases through the expansion waves and pressure decreases.

The effect of the boattail angle on pressure distribution and the drag of an axisymmetric model were studied experimentally under low-speed conditions and a conclusion of the study was that the model with a boattail angle of 14° has the lowest drag (Tran, et al., 2019). Results of a study about the drag trend and flow behaviour of axisymmetric models with conical boattails under subsonic and supersonic conditions by using a numerical approach show that the minimum drag is around 14° for subsonic flow, but this value suddenly decreases to around 7° for supersonic flow (Tran, et al., 2023).

Aerodynamic problems can be solved using different methods: theoretical, experimental and empirical, or their combinations. Theoretical methods are based on the application of equations describing the air flow around the body. These equations are nonlinear, coupled, partial differential equations and not to have general analytical solutions (except for only a few very specialized cases). Solutions of the equations, without simplification of geometry and equations can be obtained numerically with application of CFD codes. Computational fluid dynamics (CFD) is the art of replacing the governing partial differential equations of fluid flow with numbers, and advancing these numbers in space and/or time to obtain a final numerical description of the complete flow field of interest (Anderson, 2017).

During the course of using computational fluid dynamics to determine the complete set of aerodynamic coefficients (static and dynamic) over the flight Mach numbers (Mach 0.6 to Mach 2.7), the computed base pressure in the subsonic and transonic flight regimes were found to be quite large (sometimes even greater than free stream) such that either a very small (1% of total) or negative base drag was observed. The present study investigates the cause of this phenomenon by investigating the flow in the subsonic and transonic regimes at zero angle of attack. Computations on the standard 0.50-cal geometry were conducted using multiple turbulence models, multiple computational meshes, and multiple flow solvers to validate that this is not a numerical phenomenon. Additionally, the effect of boattail and base geometry on the base drag was investigated in order to better understand the flow phenomenon leading to the reduced base drag (Silton & Dinavahi, 2008).

This study is limited to boattail geometry small changes at the body of revolution for $M > 1$. These changes include reducing the boattail angle by only 1°, increasing the boattail angle by only 1° and increasing the length of boattail by only 1 caliber. Author's approach is based on the explanation of occurrences exactly during their current status from flow visualisation for every specific case. By providing systematic research about phenomena, it aims to show the differences between the phenomena using observations. The primary purpose of the paper is to establish the influence of the boattail angle and length on the drag coefficient at transonic and supersonic speed regimes. The secondary objective is to illustrate the phenomena which occur with small changes to boattail geometry.

2. Computational Method

The current study involves analysis of flow ahead of the base of body of revolution at transonic and supersonic speeds.

Numerical simulation of the flow field around an axisymmetric body is obtained with the computational fluid dynamics software ANSYS Fluent. The working fluid is air, an ideal gas, which is modified in accordance to compressibility. Pressure and temperature of air free flow correspond to parameters of air at sea level according to the standard atmosphere ICAO (Serdarevic-Kadic & Terzic, 2019). Flow around the body is compressible and turbulent.

Discretization of spatial domain is performed by non-uniform structured mesh. Computational domain is limited to the body contour, the symmetry axis and the outer boundary. A numerical method that simultaneously solves the equation of continuity, equation of momentum and energy equation is used. This method is developed for high velocity compressible flows. Two equations k-ε model is selected for turbulence modelling.

The governing equations are linearized by implicit manner. For a given variable, the unknown value in each cell is computed using a relation that includes both existing and unknown values from neighbouring cells. Therefore each unknown will appear in more than one equation in the system, and these equations must be solved simultaneous to give the unknown quantities.

3. Model geometry

Projectile 155 mm M107 is selected as basic body. Sketch of a half of the body is shown at Fig. 2.

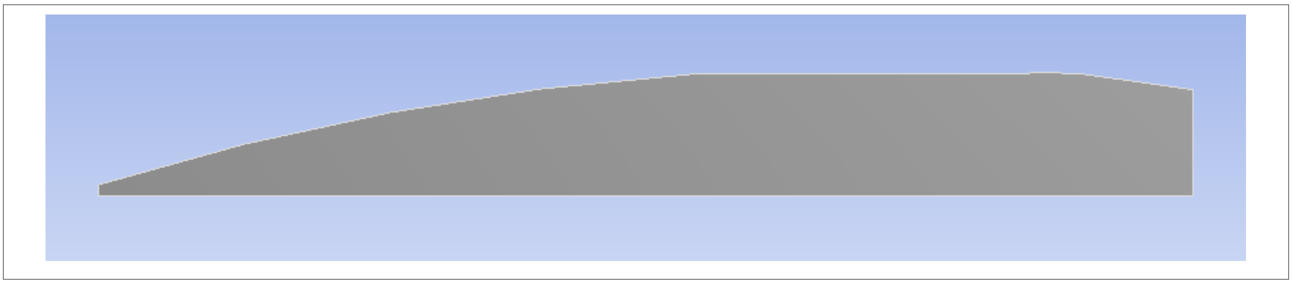

Fig. 2. Sketch of a half of basic body

Nose of the projectile has the shape of a secant ogive, with fineness of ogive $\lambda_n = 2.43$ and the radius of nose is 10.78 calibres. The afterbody of the projectile has the shape of a blunt cone with fineness ratio $\lambda_{bt} = 0.45$ and angle $\theta_{bt} = 8°$ Total length (in calibres) of projectile is $\lambda = 4.54$.

Computational domain is shown at Fig. 3. Boundaries are set to the exterior contour of domain as follow. Wall boundary, which is used to delimit the regions of fluid and solid, is set to body contour and it is divided to nose, cylinder, boattail and base.

Axis boundary is used as central line of axisymmetric geometry. The pressure far field boundary, which is used for modelling of compressible free flow parameters at the infinity, is set on the outer boundary of computation domain.

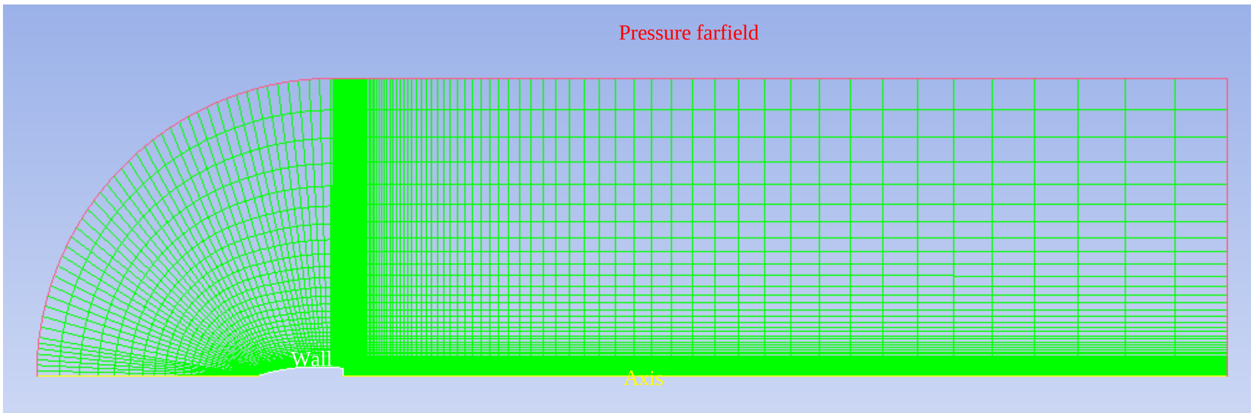

Fig. 3. Computational domain with boundaries.

Distance from the outer boundary to the wetted surface of the body is 3 body lengths and horizontal distance from the outer boundary to the body base is 10 body lengths.

Solution of Navier-Stokes equations was done by using two dimensional axisymmetric density based solver.

Based on the experimental values of the drag coefficient of projectile 155 mm M107, the model of computation is confirmed (Tab. 1). Differences between experimental and numerical values are less than 1.83%.

Mach number	Drag coefficient		Difference (%)
	CFD	(McCoy, 2009)	
1.1	0.3904	0.391	0.15
1.2	0.379	0.384	1.3
1.5	0.3371	0.341	1.14
2	0.2847	0.29	1.83

Tab. 1. Drag coefficient of basic body

Three boattail geometries (Fig. 3.) with small changes related to basic configuration are considered: a) boattail angle $\theta_{bt} = 7°$ (mod I), b) boattail angle $\theta_{bt} = 9°$ (mod II) and c) extended length of boattail $\lambda_{bt} = 0.95$ (mod III).

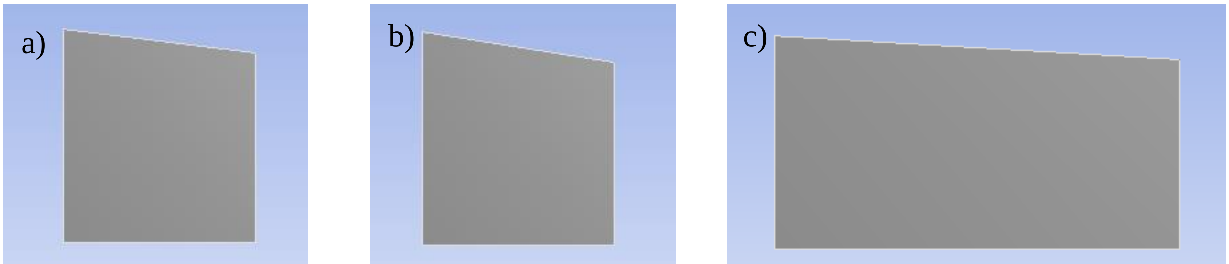

Fig. 4. Sketch of a half of boattail: a) $\theta_{bt} = 7°$, b) $\theta_{bt} = 9°$and c) $\lambda_{bt} = 0.95$

Rear part with decreased angle (Fig. 4. a)) has diameter of base $d_B = 0.889\ cal$, with increased angle (Fig. 4. b)) has diameter of base $d_B = 0.857\ cal$ and with increased length (Fig. 4. c)) has diameter of base $d_B = 0.733\ cal$. The basic body has diameter of base $d_B = 0.873\ cal$.

4. Results and discussion

Simulations have been made for modified bodies with different boattail geometry (with boattail angles 7° and 9° and original fineness of boattail and with boattail length 0.95 calibre and original boattail angle), for $M = 1.1$ and $M = 2$, with zero angle of attack.

By solving the equations that describe the airflow around the projectile and applying computational fluid dynamics, it is possible to display flow field images around the projectile in addition to the aerodynamic coefficients, allowing for the analysis of phenomena that occur during exposure of the body to air flow. Disturbances cannot propagate upstream at flow velocity $M > 1$, so only occurrences around the boattail and the base will be analysed.

Drag coefficients of base C_{DB} and drag coefficients of boattail C_{Dbt} for original body, mod I, mod II and mod III are presented at Table 2.

M	Drag coefficient							
	Original body $\theta_{bt} = 8°$ $l_{bt} = 0.45$		Mod I $\theta_{bt} = 7°$ $l_{bt} = 0.45$		Mod I $\theta_{bt} = 9°$ $l_{bt} = 0.45$		Mod I $\theta_{bt} = 8°$ $l_{bt} = 0.95$	
	C_{DB}	C_{Dbt}	C_{DB}	C_{Dbt}	C_{DB}	C_{Dbt}	C_{DB}	C_{Dbt}
1.1	0.133	0.139	0.134	0.071	0.118	0.158	0.061	0.115
2	0.109	0.054	0.105	0.042	0.101	0.065	0.055	0.084

Tab. 2. Drag coefficients of the base and boattail for the analysed cases.

For $M = 1.1$, the highest base drag coefficient was obtained with the modified body (mod I), which has a reduced angle of the rear cone. The lowest drag coefficient value at the transonic speed is observed for the body with the extended rear cone, designated as mod III.

In the supersonic range, for $M = 2$, the lowest base drag coefficient is observed with the body featuring an extended rear cone (mod III), and compared to the original projectile, this coefficient is nearly halved.

For $M = 2$, the lowest drag coefficient of the boattail was obtained with the modified body which has a reduced angle of the rear cone (mod I). The highest drag coefficient of the rear part was recorded in the transonic regime, at a Mach number close to 1, with the modified projectile that has an increased angle of the rear cone (mod II).

For each considered case of body modification and selected Mach numbers, velocity fields expressed through Mach number contours were generated, allowing for the visualization of key aerodynamic phenomena. The images are grouped by velocity of free flow.

At a Mach number around 1, the flow is characterized by a combination of subsonic and supersonic regions, as well as compression and expansion zones. In this regime, the formation of shock waves becomes crucial for the aerodynamic characteristics of the body.

Figure 5 shows the velocity fields for each analysed bodies at a free flow velocity of 1.1 Mach. A common feature in all the velocity field representations is the appearance of a bow shock wave in front of the projectile, behind which the flow becomes locally subsonic, as well as the presence of a weaker shock wave in front of the projectile's rotating band. At the transition from the cylindrical part to the conical rear part, expansion waves are created, causing the flow to redirect and follow the external contour of the projectile.

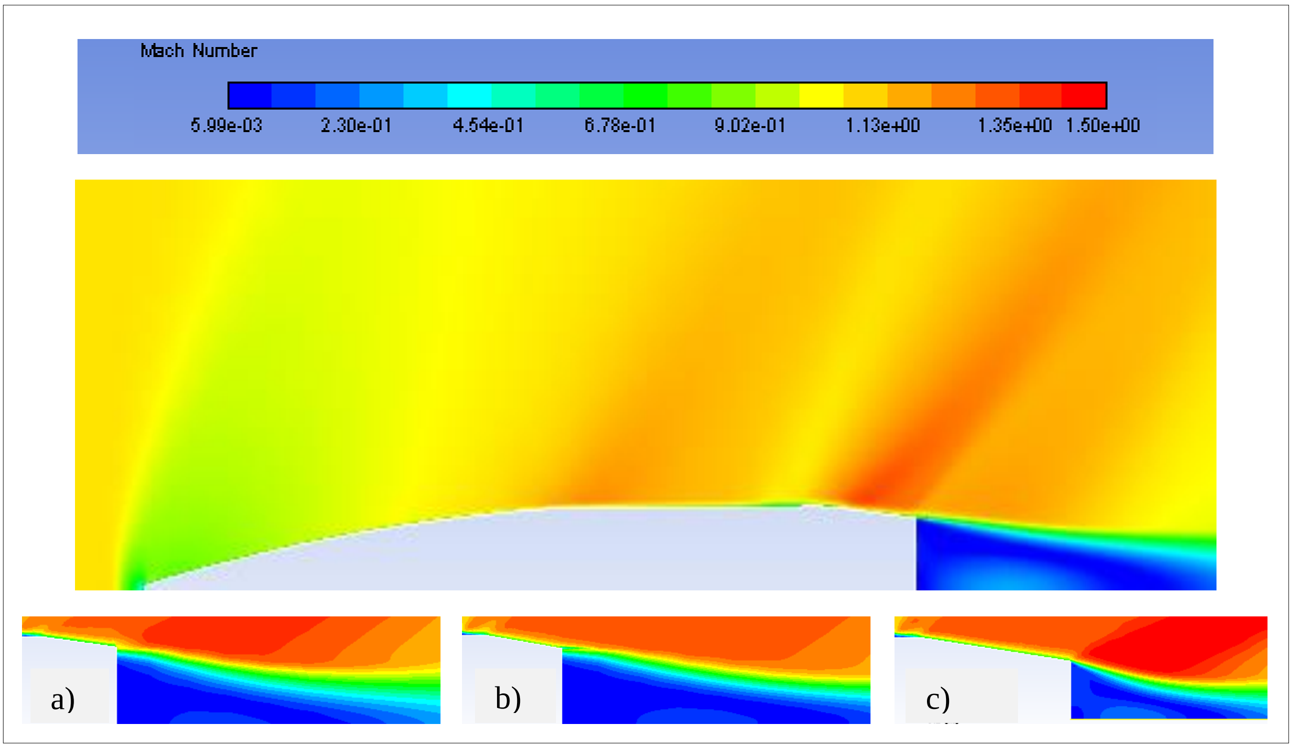

Fig. 5. Flow fields by contour Mach number for considered cases at $M = 1.1$

By comparing the velocity fields around the rear part of the body between the original body and mod I (Fig. 5. a)), an increase in flow velocity can be observed through the fan of expansion waves at the rear cone of the projectile. With the reduction of the rear cone angle by 1°, this increase in velocity is less pronounced than in the case of the rear cone of the original body. The extended boundary layer gradually approaches the axis of symmetry, resulting in a lower drag coefficient for the rear part of the body and a slight difference in the base drag coefficient.

In the case of mod II (Fig. 5. b)), with an increased angle of the rear cone by 1°, the velocity field in the area around the rear part of the body shows a significant difference compared to the velocity field around the basic body.

The flow velocity through the expansion waves does not exceed the value of 1.35 Mach at the rear cone, resulting in higher pressure on the rear part of the body, and consequently a greater drag coefficient at the boattail. The pressure acting on the base of the body is lower than in the case of original body, which means that the pressure coefficient is higher, but, since the base area is smaller, this results in a lower base drag coefficient.

From flow velocity around body marked as mod III (Fig. 5.c)), it can be observed that increasing the fineness of the rear cone improves the flow adjustment to the surface of the rear part of the body. It is also noted that there is no change in airflow velocity over the rear cone, indicating that the pressure acting on the rear cone remains constant from point to point. At the exit edge of the body's base, the flow accelerates through a fan of expansion waves, reducing the recirculating region behind the base.

The velocity fields for the analysed bodies under supersonic flow at a free-stream velocity of 2 Mach is shown at Fig. 6. Shock wave is visible at the tip of the body, through which the flow velocity drops immediately behind the shock wave. At the transition from the cylindrical part to the rear part, expansion waves are formed, causing the flow to accelerate and bend to follow the contour of the rear section. At the edge of the base of the body, a fan of expansion waves is formed, leading to a decrease in pressure.

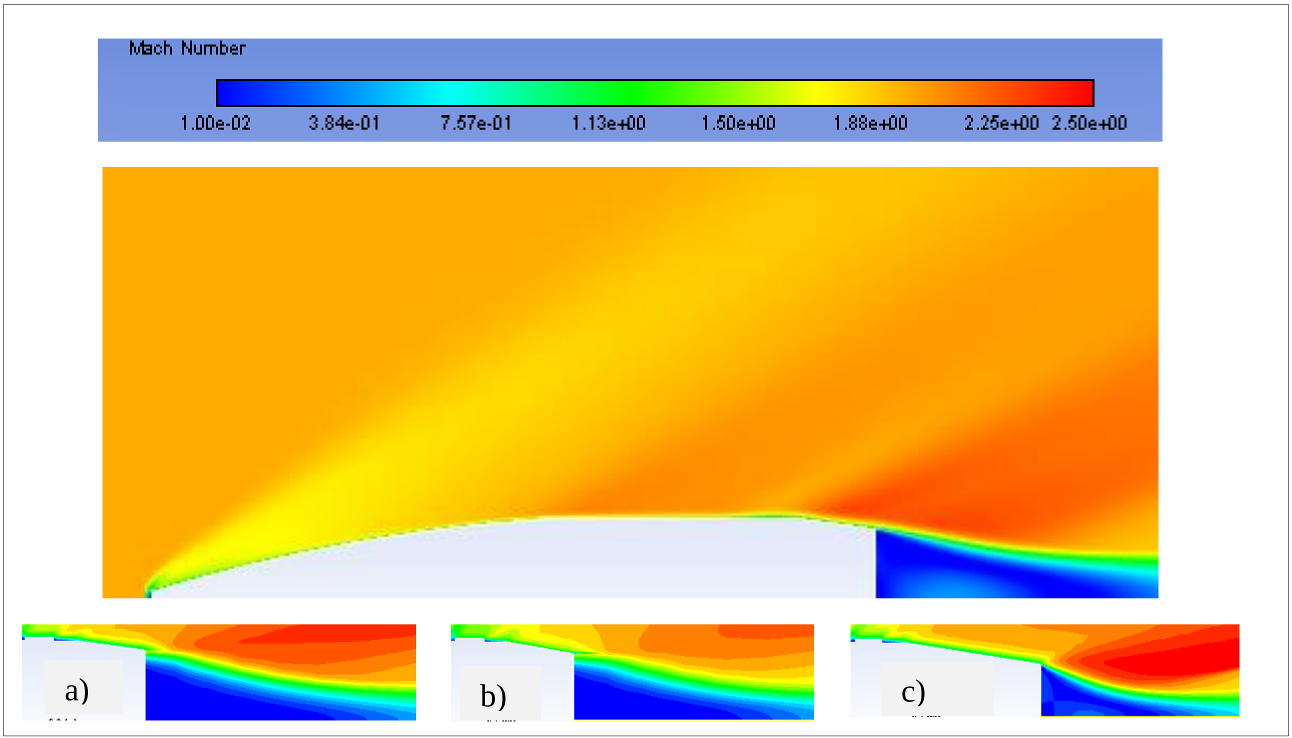

Fig. 6. Flow fields by contour Mach number for considered cases at $M = 2$

By comparing the velocity field of original body in Fig. 6. and the velocity field of modified body in Fig. 6.a), it can be observed that the flow around the rear part accelerates earlier in the case of modified body, while a gentler deflection of the flow towards the axis of symmetry is visible behind the body when the angle of the rear cone is 7° (mod I).

The consequences of this are lower drag coefficients for both the rear part and the base in the case of the modified body.

By comparing the velocity field around original body and mod II, it can be observed that the flow moves more slowly over the rear part when the angle is increased by 1°, resulting in higher pressure and a greater drag coefficient for the rear part of modified body II. In the case of the modified body shown in Fig. 6.b), a zone can be seen behind the body with more gradual changes in pressure and a less pronounced recirculating region, leading to a lower base drag coefficient compared to the drag coefficient of the basic body.

The velocity field around modified body III is shown in Fig. 6.c). As a result of the flow simulation for this case, the drag coefficient of the rear cone was found to be higher than that of the rear cone of the basic body. This is attributed to the size of the surface on which the pressure acts. The drag coefficient of the base for the modified body is nearly half as much for two reasons: first, due to the reduced surface area of the base subjected to the underpressure and second, because of the greater increase in flow velocity through the fan of expansion waves at the edge of the base of the body, which directly influences the size of the recirculating region behind the base.

5. Conclusion

Numerical computations have been made for the bodies at transonic and supersonic speeds. A basic body had a cone rear part with the length of 0.45 cal and angle 8° and the numerical model is confirmed by experimental drag coefficient.

The bodies whose external contours differ only in the geometry of the rear part are considered in the study. The following cases of changing the geometry of the rear part were considered:

- With boattail angle of 7° and length of boattail 0.45 calibre (mod I),
- With boattail angle of 9°and length of boattail 0.45 calibre (mod II), and
- With boattail angle of 8° extended length of boattail to 0.95 calibre (mod III)

Results of simulation are analysed in relation to the image of the velocity field of the basic body. Changes in flow velocity are observed through the fan of expansion waves at the rear part (cone) of the body.

Results show that the lowest drag coefficient of boattail is achieved with boattail angle of 7° and boattail length of 0.45 calibre for supersonic flow. The lowest base drag is achieved when boattail is elongated for 0.5 calibre. For the small change of boattail geometry the base drag coefficient decreases by approximately 50%.

Results show that the lowest drag coefficient is achieved with longer boattail, but the optimal geometry for minimum drag has the body with boattail angle of 7° and boattail length of 0.45 cal for supersonic flow.

If the boattail is too steep, the air flow will not remain attached and will separate from the body and it would lead to an increase in drag. The lowest drag coefficient is achieved with longer boattail, but it can result in instability of body which requires additional research.

6. References

Anderson, J. D. (2017). Fundamentals of aerodynamics, McGraw-Hill Education.

Bournot, H., Daniel, E. and Cayzac, R. (2006). Improvements of the base bleed effect using reactive particles, International Journal of Thermal Sciences, Vol. 45, No. 11, pp. 1052-1065.

Litz, B. (2015). Applied ballistics for long range shooting, Applied Ballistics, LLC.

Mcauliffe, B. R. & Wall, A. S. (2016). Aerodynamic Performance of Flat-Panel Boattails and Their Interactive Benefits with Side-Skirts, SAE International Journal of Commercial Vehicles, Vol. 9, No. 2, pp. 70-82

McCoy, R. (2009). Modern exterior ballistics: The Launch and Flight Dynamics of Symmetric Projectiles, Schiffer Military History.

Sahu, J. & Heavey, K. R. (1997). Numerical Investigation of Supersonic Base Flow with Base Bleed, Journal of Spacecraft and Rockets, Vol. 34, No. 1, pp. 62–69.

Serdarevic-Kadic, S & Terzic, J. (2019). Effects of base shape to drag at transonic and supersonic speeds by CFD, Chapter 06 in DAAAM International Scientific Book 2019, pp. 071-080, B. Katalinic (Ed.), Published by DAAAM International, ISBN 978-3-902734-24-2, ISSN 1726-9687, Vienna, Austria

Silton, S. & Dinavahi, S. (2008). Base Drag Considerations on a 0.50-caliber Spinning Projectile, In: 26th AIAA Applied Aerodynamics Conference, Honolulu, Hawaii

Suliman, M. A.; Mahmoud, O. K.; Al-Sanabawy, M.A. & Abdel-Hamid, O. E. (2009) Computational Investigation of Base Drag Reduction for a Projectile at Different Flight Regimes, In: 13th International Conference on Aerospace Sciences & Aviation Technology, Military Technical College, Kobry Elkobbah, Cairo, Egypt

Tran, T. H., Dao, C. T., Le, D. A., Pham, V. K., Do, V. M. & Nguyen, T. M. (2023) Aerodynamic drag of axisymmetric models with different boattail angles under subsonic and supersonic flow conditions. Journal of Mechanical Science and Technology, Vol. 37, No. 12, pp. 6523–6535.

Tran, T. H. Ambo, T., Chen, L., Nonomura T. & Asai K. (2019). Effect of Boattail Angle on Pressure Distribution and Drag of Axisymmetric Afterbodies under Low-Speed Conditions, Transactions of the Japan Society for Aeronautical and Space Sciences, Vol. 62, No. 4, pp. 219–226.